Pergamon

Int. J. Heat Mass Transfer. Vol. 37, No. 8, pp. 1235–1255, 1994

0017–9310/94 $7.00 + 0.00

0017–9310(93)E0014–8

Buoyancy induced flow transition in mixed convective flow of air through a bottom heated horizontal rectangular duct

C. C. HUANG and T. F. LIN

Department of Mechanical Engineering, National Chiao Tung University, Hsinchu, Taiwan, R.O.C.

(*Received* 15 *December* 1992 *and in final form* 11 *October* 1993)

Abstract—A detailed numerical simulation was carried out to study the buoyancy induced flow transition in a mixed convective flow of air through a bottom heated horizontal rectangular duct. The unsteady three-dimensional Navier–Stokes and energy equations were directly solved by a higher order finite difference numerical scheme without using any turbulence modeling. Results were particularly presented for $Re = 500$ and $A = 2$ covering a wide range of Gr/Re^2 from steady laminar longitudinal vortex flow to unsteady chaotic flow. The results indicate that the increasing buoyancy causes the steady laminar flow for $Gr/Re^2 < 4$ to become a periodic laminar flow for $4 \leqslant Gr/Re^2 < 19$, then to a quasiperiodic flow for $19 \leqslant Gr/Re^2 < 25$ and finally to a chaotic flow in the downstream for $25 < Gr/Re^2 \leqslant 40$. Thus, the buoyancy induced laminar to turbulent flow transition follows the Ruelle–Taken route. An empirical equation was proposed to correlate the locations for Hopf bifurcation.

INTRODUCTION

BUOYANCY driven secondary flow in a forced laminar flow through a bottom heated horizontal rectangular duct can cause significant heat transfer enhancement and flow transition to turbulence when the buoyancy is high enough. The understanding of thermal and flow characteristics in this buoyancy induced vortex flow is important in the design of compact heat exchangers [1], cooling of microelectronic equipments [2], and chemical vapor deposition process [3]. Accordingly, a number of experimental, theoretical and numerical studies have been carried out to investigate this problem in the literature.

The condition for the inception of the secondary vortex flow (onset of thermal instability) driven by the upward buoyancy receives considerable attention. In a horizontal parallel plate channel (approximately a large aspect ratio rectangular duct) with the bottom plate at a higher uniform temperature than the top one by ΔT, the critical Rayleigh number for the appearance of the vortex flow is around 1708, as predicted from experimental measurement [4–9] and linear stability theory [4]. Beyond this critical Rayleigh number, steady longitudinal vortex rolls prevails and the roll wavelength is about twice the channel height, i.e. $\lambda = 2d$. Ostrach and Kamotani [6, 7] experimentally noted that the vortex rolls become irregular as $Ra > 8000$. For $Ra > 18\,352$ they identified a second type of vortex rolls whose wavelength is only half of that for the first type vortices, i.e. $\lambda = d$. In the thermal entrance region Kamotani *et al.* [9] indicate that the heat transfer rate is affected not only by Rayleigh number but also by the buoyancy-to-inertia force ratio Gr/Re^2. In the mixed convection of nitrogen gas Rosenberger and his coworkers [10, 11] observed the unsteady vortex rolls even for Rayleigh number only slightly above the critical value of 1708. Besides, the asymmetric roll patterns were found also at low Rayleigh numbers. A flow regime map of Re vs Ra was proposed to predict the boundaries among the flow with no roll, steady and unsteady rolls. Finally, the transverse rolls were noted at very low Reynolds number by Ouazzani *et al.* [12, 13]. They also refined the regime map to include the transverse rolls.

A series of experiments have been conducted by Incropera and his coworkers [14–19] to investigate buoyancy effects of a forced air or water flow in a horizontal plane duct with the bottom and/or top plates subject to uniform heat fluxes. The onset and qualitative picture of the buoyancy driven secondary flow on the bottom plate were clearly visualized [14]. Significant improvement in heat transfer over the bottom plate was found. While over the top plate buoyancy shows little effect in the laminar flow, it results in relaminarization in the transitional and turbulent flows [15]. Their flow visualization distinctly discloses four flow regimes along the bottom plate—laminar forced convection, laminar mixed convection, transitional mixed convection, and turbulent free convection. The transition to turbulent flow was attributed to the breakdown of the vortices due to hydrodynamic instability [17]. The onset of instability

NOMENCLATURE

A aspect ratio, b/d
b, d width and height of the duct
g gravitational acceleration
Gr modified Grashof number, $g\beta q''_w d^4/kv^2$
h local convection heat transfer coefficient
k thermal conductivity
l, L dimensional and dimensionless length of the heated plate, l/d
Nu Nusselt number, hd/k
P, p_m dimensionless and dimensional dynamic pressures, $p_m/\rho\overline{w_e}^2$
Pr Prandtl number, v/α
q''_w wall heat flux
Re Reynolds number, $\overline{w_e}d/v$
t, τ dimensional and dimensionless time, $t/(d/\overline{w_e})$
T, Θ dimensional and dimensionless temperatures, $(T-T_e)/(q''_w d/k)$
u, v, w velocity components in x, y, z directions
U, V, W dimensionless velocity components in X, Y, Z directions, $u/\overline{w_e}$, $v/\overline{w_e}$ and $w/\overline{w_e}$
x, y, z Cartesian coordinates
X, Y, Z dimensionless Cartesian coordinates, x/d, y/d and z/d
Z^+ modified Z coordinate, $Z/(Re\ Pr)$.

Greek symbols
α thermal diffusivity
β thermal expansion coefficient
v kinematic viscosity
ρ density.

Subscripts
b of bulk quantity
e values at the duct inlet
w of wall qualities.

Superscripts
$\bar{}$ average value
$*$ provisional value
n value at the n-th time step.

was found to be earlier at higher Grashof number and/or low Reynolds number [18]. In addition, a correlation for the onset points was proposed [17].

Various linear stability analyses have been carried out in the literature to predict the onset of vortex flow in the fully developed and thermal entrance regions of a horizontal flat duct heated from below by Cheng, Hwang and their colleagues [20–22]. Their earlier results [21] indicate that for $Pr \geqslant 0.7$ the flow is more stable in the thermal entrance region than in the fully developed region, but the opposite is true for $Pr \leqslant 0.2$. Recently, they noted [23] that increasing Prandtl number has a destabilizing effect on the flow for a fixed Peclet number. However, increasing Peclet or Reynolds number tends to delay the onset point.

In view of the fact that the buoyancy driven vortex flow over a bottom heated horizontal rectangular duct is three-dimensional, but steady when the Rayleigh number is slightly over the critical value and can become unsteady, transitional and even turbulent when the Rayleigh number is high enough. Direct numerical simulation of this vortex flow covering a wide range of Rayleigh number is important but relatively difficult. In the previous studies various simplifications were made to facilitate the analysis. Cheng and Hwang [23] numerically obtained the steady fully developed laminar vortex flow in isothermally heated rectangular ducts of different aspect ratios by the method of successive overrelaxation. Later, Cheng and his group [24–27] extended the analysis to the steady laminar vortex flow in the thermal entrance region with different thermal boundary conditions for large Prandtl number fluid in which the inertia force terms in the momentum equations can be neglected. They noted a minimum Nusselt number occurring at some distance from the entrance. They then moved further to include the Prandtl number and wall conduction effects [28–30] and found that the large Prandtl number assumption is valid for fluids with Pr over 10. The effects of thermal radiation was recently included by Huang *et al.* [31]. Similar computations were also performed by Incropera and his coworkers [32–36] to further consider the combined entrance effects, heating from top and bottom plates, wall heat flux distribution, and discrete wall heating. The buoyancy driven longitudinal vortex rolls were found to enhance the bottom surface heat transfer by as much as 400% over the pure forced convection [32]. In the combined entry region, the secondary flow was found to consist of longitudinal plumes and vortices that first appear near the vertical sidewalls and then propagate to the interior [33]. No attempt has been made to simulate the unsteady vortex flow at high Ra.

It should be pointed out that in the above analyses [23–36] the viscous and thermal diffusion in the streamwise direction is ignored so that the flow becomes parabolic in the flow direction and the solution can be marched in that direction, leading to tremendous saving in computer time. This approximation becomes inappropriate when the vortex flow exhibits oscillatory variations in both space and time at relatively high Rayleigh numbers. Besides, it is also inapplicable to the cases with the Reynolds or Peclet number below 100. In a preliminary attempt the pres-

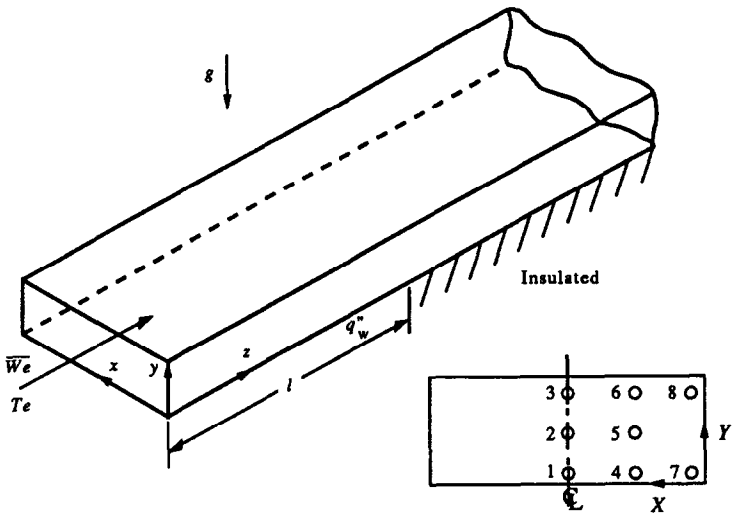

FIG. 1. Schematic of the physical system and the detection points at a cross section. (The X and Y coordinates at various points are as follows: point 1-(1,0.06), 2-(1,0.5), 3-(1,0.92), 4-(0.48,0.08), 5-(0.48,0.5), 6-(0.48,0.92), 7-(0.16,0.08), 8-(0.16,0.92).)

ent study intends to develop a numerical algorithm to accurately predict the steady and time periodic, fully elliptic, mixed convective vortex flow in a bottom heated horizontal rectangular duct. Figure 1 shows the schematic of the system to be investigated along with the coordinate system chosen. Initially at $t < 0$, the flow is fully developed and isothermal at T_e in a thermally well insulated horizontal rectangular duct. At time $t = 0$ a uniform heat flux q''_w is suddenly imposed at the bottom plate over a finite length l and maintained at this level thereafter. The initially unidirectional steady flow is significantly modified as the heating level is high enough so that the first critical Rayleigh number (the onset of vortex flow) and second critical Rayleigh number (the appearance of time periodic flow) are exceeded. The evolution of these complicated flows will be carefully simulated.

MATHEMATICAL FORMULATION

Basic equations describing the unsteady mixed convective flow of a Boussinesq fluid in a bottom heated horizontal rectangular duct are

$$\frac{\partial U}{\partial X}+\frac{\partial V}{\partial Y}+\frac{\partial W}{\partial Z}=0 \tag{1}$$

$$\frac{\partial U}{\partial \tau}+U\frac{\partial U}{\partial X}+V\frac{\partial U}{\partial Y}+W\frac{\partial U}{\partial Z}=-\frac{\partial P}{\partial X}+\frac{1}{Re}\left[\frac{\partial^2 U}{\partial X^2}+\frac{\partial^2 U}{\partial Y^2}+\frac{\partial^2 U}{\partial Z^2}\right] \tag{2}$$

$$\frac{\partial V}{\partial \tau}+U\frac{\partial V}{\partial X}+V\frac{\partial V}{\partial Y}+W\frac{\partial V}{\partial Z}=-\frac{\partial P}{\partial Y}+\frac{1}{Re}\left[\frac{\partial^2 V}{\partial X^2}+\frac{\partial^2 V}{\partial Y^2}+\frac{\partial^2 V}{\partial Z^2}\right]+\frac{Gr}{Re^2}\theta \tag{3}$$

$$\frac{\partial W}{\partial \tau}+U\frac{\partial W}{\partial X}+V\frac{\partial W}{\partial Y}+W\frac{\partial W}{\partial Z}=-\frac{\partial P}{\partial Y}+\frac{1}{Re}\left[\frac{\partial^2 W}{\partial X^2}+\frac{\partial^2 W}{\partial Y^2}+\frac{\partial^2 W}{\partial Z^2}\right] \tag{4}$$

$$\frac{\partial \theta}{\partial \tau}+U\frac{\partial \theta}{\partial X}+V\frac{\partial \theta}{\partial Y}+W\frac{\partial \theta}{\partial Z}=\frac{1}{Re\,Pr}\left[\frac{\partial^2 \theta}{\partial X^2}+\frac{\partial^2 \theta}{\partial Y^2}+\frac{\partial^2 \theta}{\partial Z^2}\right] \tag{5}$$

subject to the following initial and boundary conditions:

$$\text{at } \tau = 0 \text{ or } Z = 0,\ U = V = \theta = 0$$

$$W=\left(\frac{m_1+1}{m_1}\right)\times\left(\frac{m_2+1}{m_2}\right)[1-(|2Y-1|)]^{m_2}\left[1-\left(\left|\frac{2X}{A}-1\right|\right)^{m_1}\right] \tag{6}$$

where the above inlet velocity profile is assumed as fully developed with the values of the constants m_1 and m_2 depending on the aspect ratio A [37].

$$\text{At } Z = 2L,\ \frac{\partial U}{\partial Z}=\frac{\partial V}{\partial Z}=\frac{\partial \theta}{\partial Z}=\frac{\partial W}{\partial Z}=0 \tag{7}$$

$$\text{at } Y = 0 \text{ and } Z \leqslant L,\ \frac{\partial \theta}{\partial Y}+1 = U = V = W = 0 \tag{8}$$

$$\text{at all other surfaces},\ \frac{\partial \theta}{\partial n} = U = V = W = 0 \tag{9}$$

where n is a unit normal to a surface. The above equations are in terms of the nondimensional variables defined in the Nomenclature.

Note that in the above formulation an insulated section of length l_1 is added to the exit end of the

heated section to facilitate the prescription of the out-flow boundary conditions in the present elliptic flow analysis. The exact out-flow conditions should be given at $Z \to \infty$. In actual computation l_1 is chosen to be long enough so that the predicted flow in the heated section is independent of its size. In the program tests several values of l_1 were used and we chose $l_1 = l$. No insulated section is added to the inlet end since the upstream diffusion from the inlet can be neglected for $Re \gg 1$ which is the situation considered here.

The local Nusselt number measuring the convective heat transfer from the plate to the flow in the heated duct is defined as

$$Nu = \frac{h \cdot d}{k} = \frac{q''_w}{T_w - T_b}\frac{d}{k} = \frac{1}{\theta_w - \theta_b}. \quad (10)$$

The spanwise averaged Nusselt number is defined as

$$\overline{Nu(Z)} = \frac{q''_w}{\frac{1}{b}\int_0^b (T_w(x,z) - T_b(z))\,dx}\frac{d}{k}. \quad (11)$$

SOLUTION METHOD

In view of the complex unsteady three-dimensional mixed convective vortex flow to be simulated, a highly efficient and accurate numerical scheme is needed. After comparing a number of available methods in the open literature, we chose the projection method [38, 39] combining with the higher order finite difference spatial discretization to solve the Navier–Stokes equations in primitive form on a staggered grid system. This splitting (fractional step) method consists of two steps. First, a provisional velocity field $\mathbf{V}^*$ is explicitly computed ignoring the pressure gradient,

$$\frac{\mathbf{V}^* - \mathbf{V}^n}{\Delta\tau} + (\mathbf{V}^n \cdot \nabla)\cdot \mathbf{V}^n - \frac{1}{Re}\nabla^2 \mathbf{V}^n - \mathbf{B} = 0 \quad (12)$$

where Re is the Reynolds number of the flow and $\mathbf{B}$ is the buoyancy force. Then, it is corrected by including the pressure effect and by enforcing the mass conservation at time step $n+1$,

$$\frac{\mathbf{V}^{n+1} - \mathbf{V}^*}{\Delta\tau} + \nabla P^{n+1} = 0 \quad (13)$$

and

$$\nabla \cdot \mathbf{V}^{n+1} = 0. \quad (14)$$

Substituting equation (13) into equation (14) yields the Poisson equation for pressure,

$$\nabla^2 P^{n+1} = \frac{1}{\Delta\tau}\nabla \cdot \mathbf{V}^*. \quad (15)$$

In discretizing the above equations, centered difference is used to approximate all the derivatives except the convective terms. To enhance numerical stability and to yield accurate results for the complicated flow and thermal evolution studied here, a third-order upwind scheme developed by Kawamura *et al.* [40] is employed to discretize these convective terms. Specifically for a typical convective term

$$u\left.\frac{\partial f}{\partial x}\right|_i \approx u\frac{-f_{i+2} + 8f_{i+1} - 8f_{i-1} + f_{i-2}}{12\Delta x} + |u|\frac{f_{i+2} - 4f_{i+1} + 6f_i - 4f_{i-1} + f_{i-2}}{4\Delta x} \quad (16)$$

where f denotes velocity components or temperature. Additionally, the diffusive terms are approximated by a fourth-order central difference [41]. For instance

$$\frac{\partial^2 f}{\partial x^2} \approx (-f_{i+2} + 16f_{i+1} - 30f_i + 16f_{i-1} - f_{i-2})/12(\Delta x)^2. \quad (17)$$

Time advancement may be done either implicitly or explicitly. The first-order Euler explicit scheme was employed since it was easy to implement. It has much lower computational cost per time step, and requires much less computer memory allocation than any equivalent implicit implementation. We also found that the first-order scheme was sufficiently accurate to resolve the smallest physical time scale. The stability of the scheme is limited by the requirement that the Courant number be less than unity (Anderson *et al.* [42]). To insure the numerical convergence, the Courant number is set below 0.5 in the computation, which leads to

$$\Delta\tau < 0.5 \cdot \text{minimum}\left(\frac{\Delta X}{U_{max}}, \frac{\Delta Y}{V_{max}}, \frac{\Delta Z}{W_{max}}\right). \quad (18)$$

The sequence of numerical operation is as follows:

(1) Explicitly calculate $\mathbf{V}^*$ from equation (12).

(2) Solve the pressure equation (15) for P^{n+1} by the vectorized Gauss–Seidel method with successive over-relaxation. Solution for the pressure is considered as convergent when the mean relative pressure difference between two consecutive iterations is below 10^{-4}, that is

$$\sum_{i,j,k}\frac{|(P^{n+1}_{i,j,k})^{m+1} - (P^{n+1}_{i,j,k})^m|}{|(P^{n+1}_{i,j,k})^{m+1}|(I \cdot J \cdot K)} < 10^{-4} \quad (19)$$

where i, j, k are respectively the indices of the nodes in the X, Y and Z directions, m is the iteration number and I, J and K are the total numbers of nodes in the X, Y and Z directions, respectively.

(3) Explicitly calculate the desired velocity field at the new time step, $\mathbf{V}^{n+1}$, from equation (13). A uniform grid is placed in the computational domain with $\Delta X = A/I$, $\Delta Y = 1/J$ and $\Delta Z = 2L/K$. I, J and K are varied from 31 to 51 depending on the particular set of parameters to be investigated.

To verify the proposed numerical scheme, a series of program tests were conducted. First, the predicted spanwise average Nusselt number variations with the axial coordinate for the pure forced convection ($Gr/Re^2 = 0$) of air in a rectangular duct were found to be in excellent agreement with the numerical and

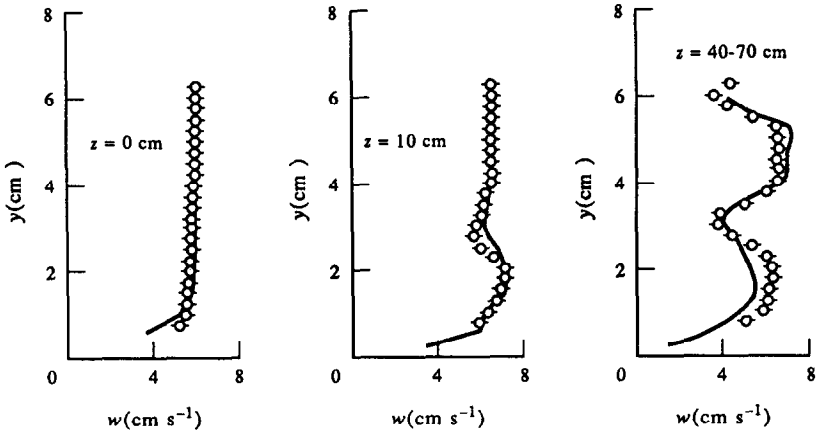

FIG. 2. Comparison of the predicted streamwise velocity profiles (solid lines) at selected cross sections at $X = A/2$ with the data of Chiu and Rosenberger [10] (open circles) for $Pr = 0.7$, $Re = 44.8$, $Gr/Re^2 = 3.43$ and $A = 10$.

experimental results of Incropera *et al.* [33,18]. Then, the steady mixed convection of nitrogen in a high aspect ratio rectangular duct with its bottom wall at a higher uniform temperature over its top wall was simulated. The comparison of the computed axial velocity profiles for a typical case with $Pr = 0.7$, $Re = 44.8$, $Gr/Re^2 = 3.43$ and $A = 10$ with the experimental data of Chiu and Rosenberger [10] given in Fig. 2 shows good agreement. Similar comparison was also made in Fig. 3 to test the data of Maughan and Incropera [19] for combined entrance mixed convection. The predicted $\overline{Nu}(\bar{z})$ at $\tau = 100$ corresponds to the results at statistical state. The agreement in the overall flow pattern and local Nusselt number is also good except that earlier appearance of the vortex rolls is predicted in this study. Finally, grid test were performed. Results from this test are compared in Fig. 4 for the spanwise average Nusselt number at various time instants for a typical case with $Pr = 0.7$, $Re = 100$, $Gr/Re^2 = 3$, $L = 20$, and $A = 2$ in which the steady state prevails at large τ. Note that the differences in the results calculated from the $31 \times 31 \times 31$, $41 \times 41 \times 41$ and $51 \times 51 \times 51$ grids are all less than 3%. Furthermore, we compare the calculated frequency of the flow oscillation for a case with a higher buoyancy at $Gr/Re^2 = 8$. Again, the differences in the results from these three grids are also less than 3%. Through these program tests, the adopted solution procedures are considered to be suitable for the present study.

RESULTS AND DISCUSSION

According to the foregoing formulation, there are five governing nondimensional groups for the problem, namely, the Prandtl number Pr, Reynolds number Re, buoyancy-to-inertia ratio Gr/Re^2, aspect ratio A, and dimensionless heating length L. Considering the complex three-dimensional oscillatory flow to be simulated, a fully parametric study is formidable. In an initial attempt in this numerical exploration, attention is focused on the effect of the buoyancy strength Gr/Re^2. In particular, Gr/Re^2 is varied from 0 to 40 with $Pr = 0.72$, $Re = 500$, $A = 2$ and $L = 20$.

Before presenting the oscillatory flow at high Gr/Re^2, we first examine the characteristics of the steady vortex flow at low buoyancy. Our predicted onset of the longitudinal vortices for various Gr/Re^2 were compaired the data of Kamotani and Ostrach [7], Kamotani *et al.* [9], Chiu and Rosenberger [10], Maughan and Incropera [19], Hwang and Cheng [21], and Lee and Hwang [22]. The results indicate that our predictions are in reasonable agreement with these data. This again supports the use of the proposed solution method for the present investigation. Steady mixed convective vortex flows for $Gr/Re^2 = 1$, 2 and 3 are shown in Fig. 5 to illustrate the flow and thermal development with the axial distance. Due to the flow being symmetric with respect to the center plane at $X = A/2$, only the isotherms on the left half and the streamlines of the secondary flow on the right half of the channel are presented together to save the limited space available for the article. An overall inspection of the results reveals that the buoyancy driven secondary flow in the form of two cross-plane recirculation cells first appear in the two lower corners in the entry portion, causing distortion in the isotherms in these regions. In three-dimensional space we have two longitudinal rolls in the duct. As the flow moves downstream, these cells gradually grow and diffuse into the core region owing to continuing action of the upward buoyancy. The secondary flow at every cross-section is dominated by these two cells. At a higher buoyancy the secondary flow is stronger and the cells are bigger. Note that based on the values of the streamfunctions the intensity of the secondary flow gets stronger as the flow moves downstream except near the exit end of the heated section.

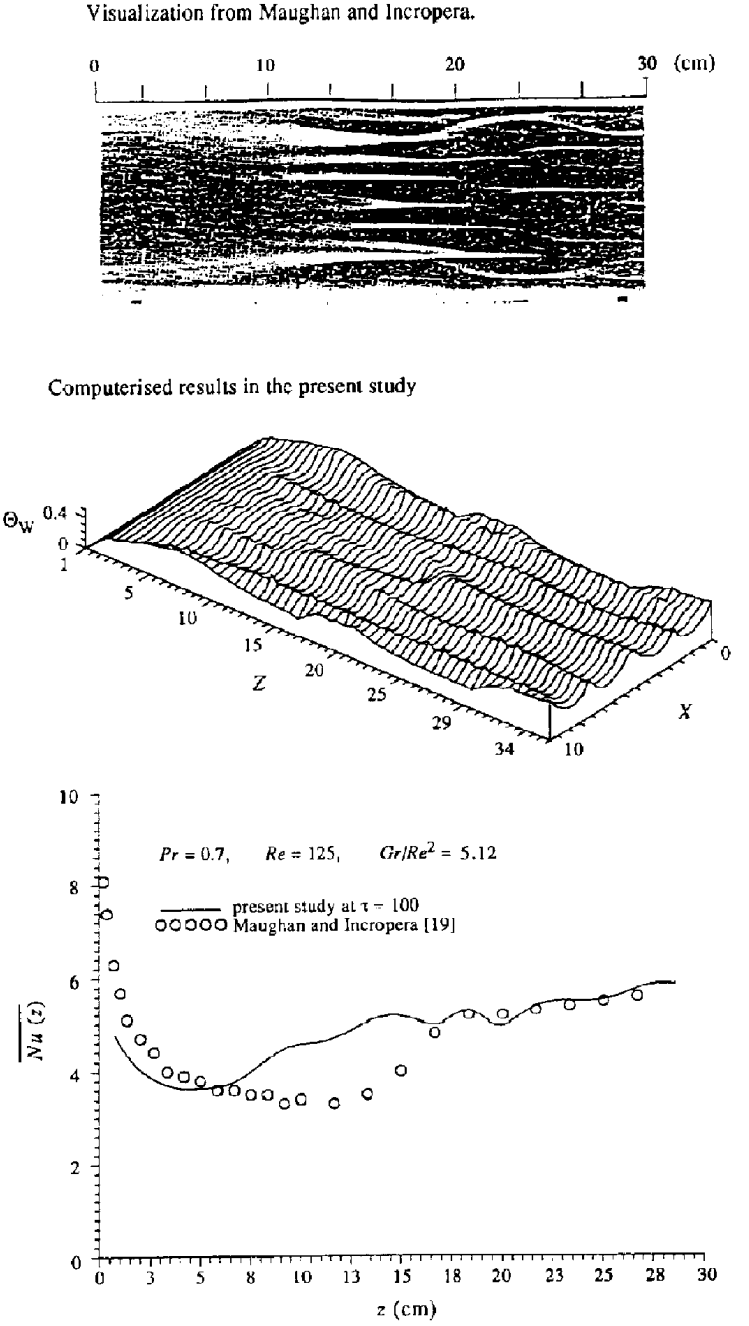

FIG. 3. Comparison of the flow pattern and spanwise average Nusselt number with the data of Maughan and Incropera [19] for $Pr = 0.7$, $Re = 125$, $Gr/Re^2 = 5.12$.

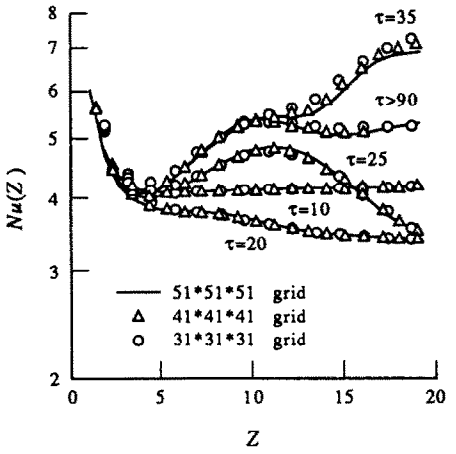

FIG. 4. Comparison of the spanwise average Nusselt number at selected instants from various grids for $Pr = 0.72$, $Re = 100$, $Gr/Re^2 = 3$, $A = 2$ and $L = 20$.

As Gr/Re^2 is raised to 4, very weak flow and thermal oscillations are noted in the trailing edge of the heated bottom plate. For $Gr/Re^2 = 5$ the flow is found to be steady in the upstream region, but becomes unsteady and oscillatory in the downstream region. Figure 6 presents three snapshots of the temperature contours and secondary flow at selected cross-sections and time instants. For clear presentation in Fig. 6 the solid and dashed lines respectively are used for cells with counter-clockwise and clockwise rotations. It is worth noting that, in addition to the vortices originating from the lower corners as that at lower Gr/Re^2, two new cells are induced in the core region near the exit end of the heated section (Fig. 6(g)). These new cells are in fact the thermals [17] driven by the upward buoyancy near the central portion of the heated bottom plate (Figs. 6(f), (g)). Checking the secondary flow intensities reveals that the newly formed cells grow quickly and later even become stronger than the original cells (Fig. 6(g)). Of particular importance is the recognition that in each half channel the cell in the central portion and the cell near the side wall are counter-rotating. Hence the flow is potentially unstable.

To further elucidate the unsteady flow characteristics for the case with $Gr/Re^2 = 5$, Fig. 7 gives the time traces of the axial velocity component W and temperature Θ at eight detection points specified in Fig. 1 at a downstream location $Z = 14.84$ after a long time when the flow has reached a statistical fluctuating state and the corresponding power spectrum densities (PSD). These time records indicate that after the initial transient the flow is in periodic oscillation. Examining the time records for U, V, W and Θ at various locations from the computer output in detail discloses that the amplitudes of the flow and temperature oscillations are position-dependent. It is of interest to note that in a given cross-section the oscillations are normally larger at locations outside the longitudinal rolls. Besides, the intensities of the oscillations do not always increase with the axial distance. In fact, they are greatly affected by the axial development of the longitudinal rolls. Inspecting the power spectrum densities, we observe a number of discrete peaks in each plot. More peaks appear for a larger Z. Comparing the frequencies of these peaks suggests that only one fundamental frequency exists irrespective of the detection points, $f_1 = 0.043$. All other frequencies are simply the harmonics of this fundamental model, which are in fact from the period doubling process [43]. To further provide the detailed information, the evolution of the secondary flow in a typical period at large τ at the cross-sections $Z = 9.03$, 11.61, 14.19, and 16.7 is shown in Fig. 8. The results for $Z = 14.19$ and 16.77 clearly show that in a certain part of the period the longitudinal vortex rolls in the core region grow in size with accompanying shrinkage in the corner cells. In another part of the period an opposite process takes place. Scrutinizing the streamfunction values above each plot evinces the considerable fluctuation in the secondary flow intensity at large Z (Fig. 8(d)).

As Gr/Re^2 is further raised to 10, flow is found to be steady in a smaller region near the leading edge of the heated plate ($Z \leqslant 6.54$) (Figs. 9(a)–(c)). It is also noted that the thermals arising from the central portion of the heated bottom plate appear at a earlier time and closer to the duct inlet. At this higher buoyancy the unsteady flow in the downstream region is still periodic, and is again characterized by a single fundamental frequency $f_1 = 0.073$. Further numerical experiments for higher buoyancies with $Gr/Re^2 = 12$, 15 and 18 manifest that the oscillatory flow is also dominated by a single fundamental mode with more harmonics at increasing buoyancy. The second fundamental mode is first seen in the downstream region ($Z \geqslant 14.84$) for $Gr/Re^2 = 19$. The flow oscillation is characterized by two fundamental frequency modes, $f_1 = 0.137$ and $f_2 = 0.203$, along with linear combinations of their harmonics and subharmonics. Thus the flow is quasi-periodic. Raising Gr/Re^2 further to 25 the flow near the trailing edge becomes chaotic.

To illustrate the flow transition from periodic to quasiperiodic and finally to chaotic states in detail, Figs. 10 and 11 respectively present the time traces of Θ and W and the corresponding phase space trajectories which characterize the relative variations of three velocity components as time proceeds for $Gr/Re^2 = 30$ at three cross-sections. The results for detection points 7 and 8 in Figs. 10(a) and 11(a) indicate that near the duct inlet ($Z = 3.23$) the flow near the side walls is entirely time periodic, as apparent from the existence of a single fundamental mode in PSD and a limit cycle in phase diagram. Away from the side wall region the flow is quasi-periodic with the appearance of two fundamental modes in the flow oscillation and a three-dimensional torus in the phase diagrams. The torus is slightly irregular at location 4. A little downstream at $Z = 7.10$ the flow in the side

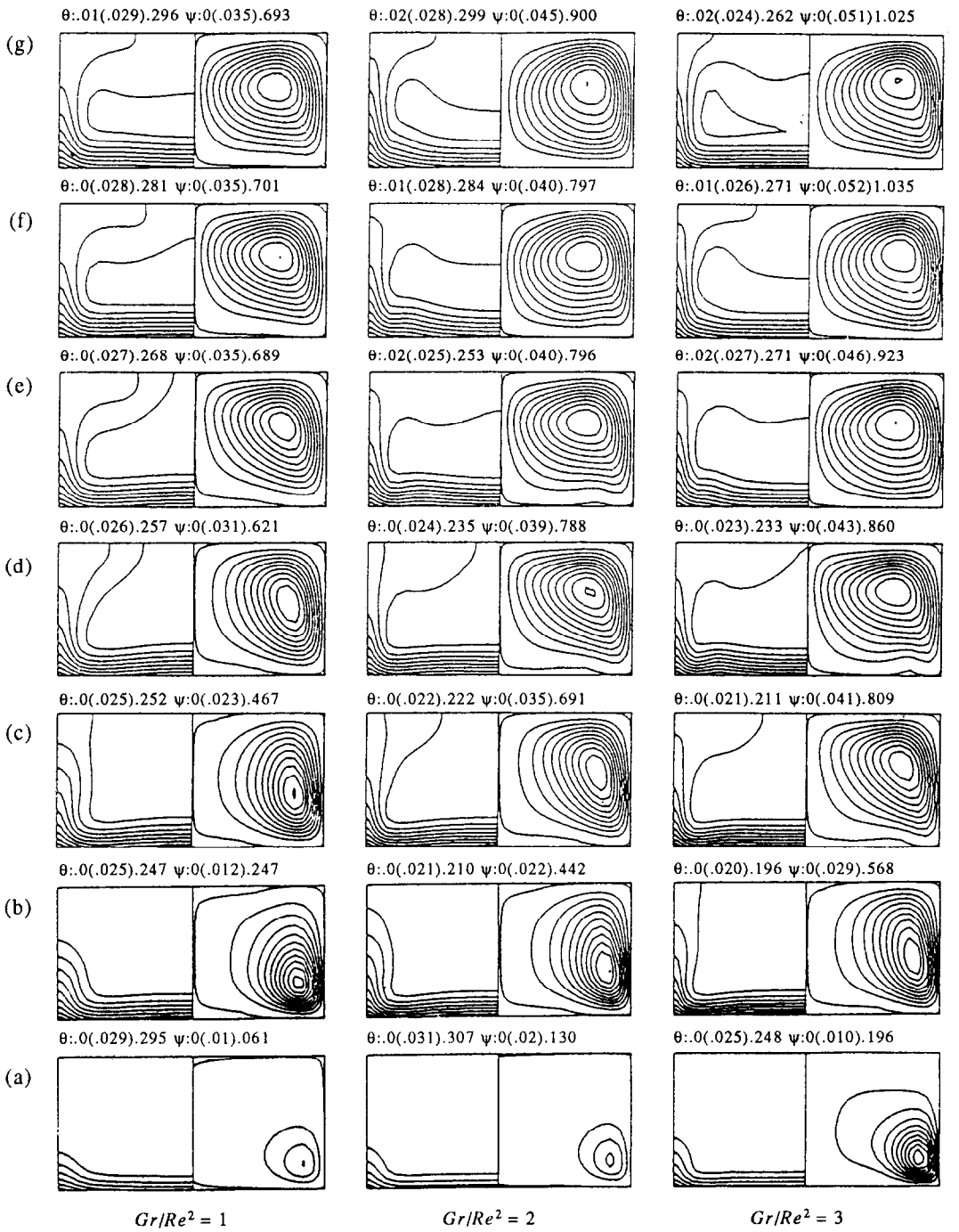

FIG. 5. Steady isotherms and streamlines at selected cross sections for $Pr = 0.72$ and $Re = 500$, $Gr/Re^2 = 1$, 2 and 3 at (a) $Z = 1.29$, (b) $Z = 3.87$, (c) $Z = 6.45$, (d) $Z = 9.03$, (e) $Z = 11.61$, (f) $Z = 14.19$, (g) $Z = 16.77$.

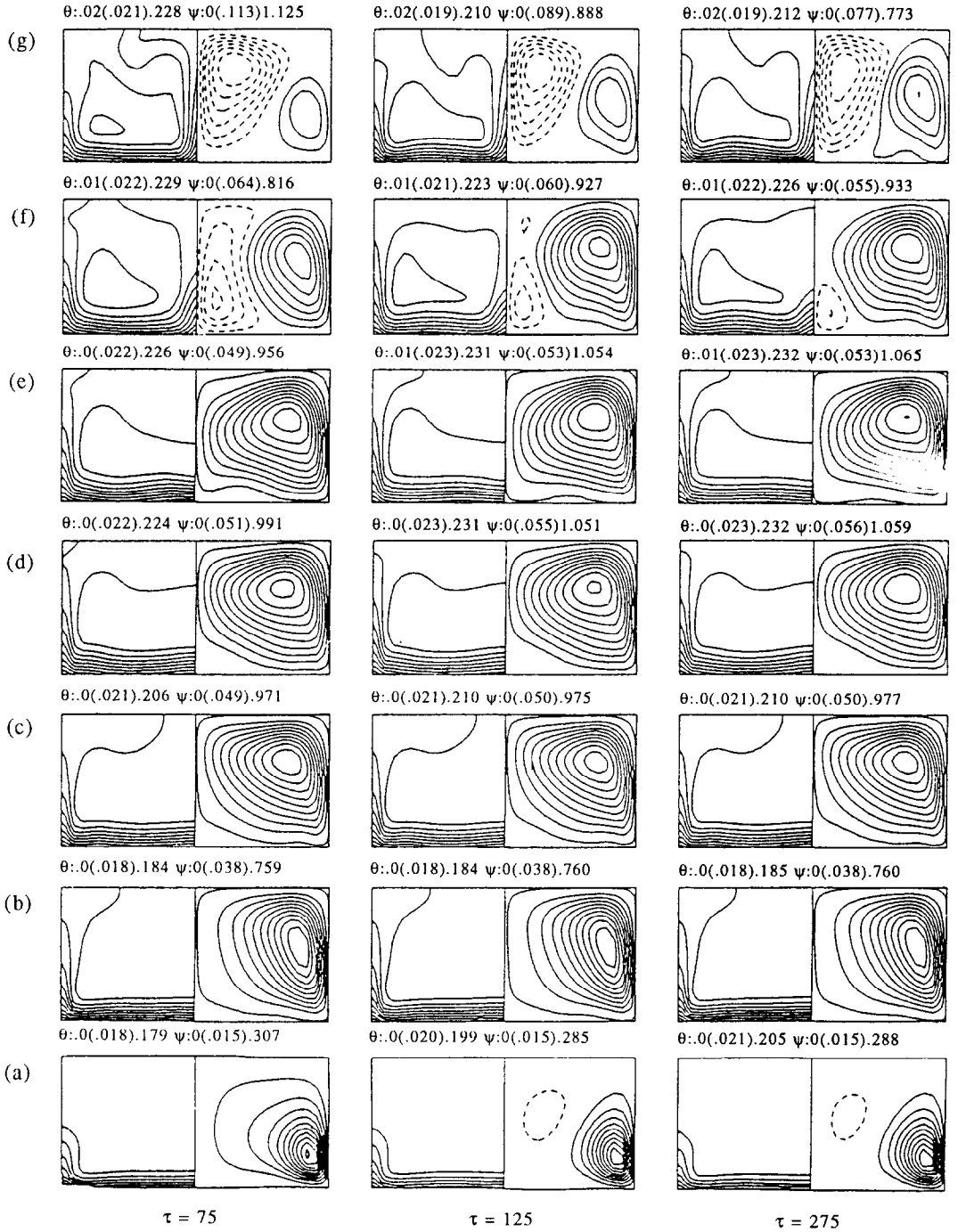

FIG. 6. Isotherms and cross-sectional streamlines for $Pr = 0.72$, $Re = 500$, $Gr/Re^2 = 5$ at (a) $Z = 1.29$, (b) $Z = 3.87$, (c) $Z = 6.45$, (d) $Z = 9.03$, (e) $Z = 11.61$, (f) $Z = 14.19$, (g) $Z = 16.77$ for $\tau = 75$, 125 and 275. (The counter-clockwise and clockwise rotating cells are respectively plotted by the solid and dash lines.)

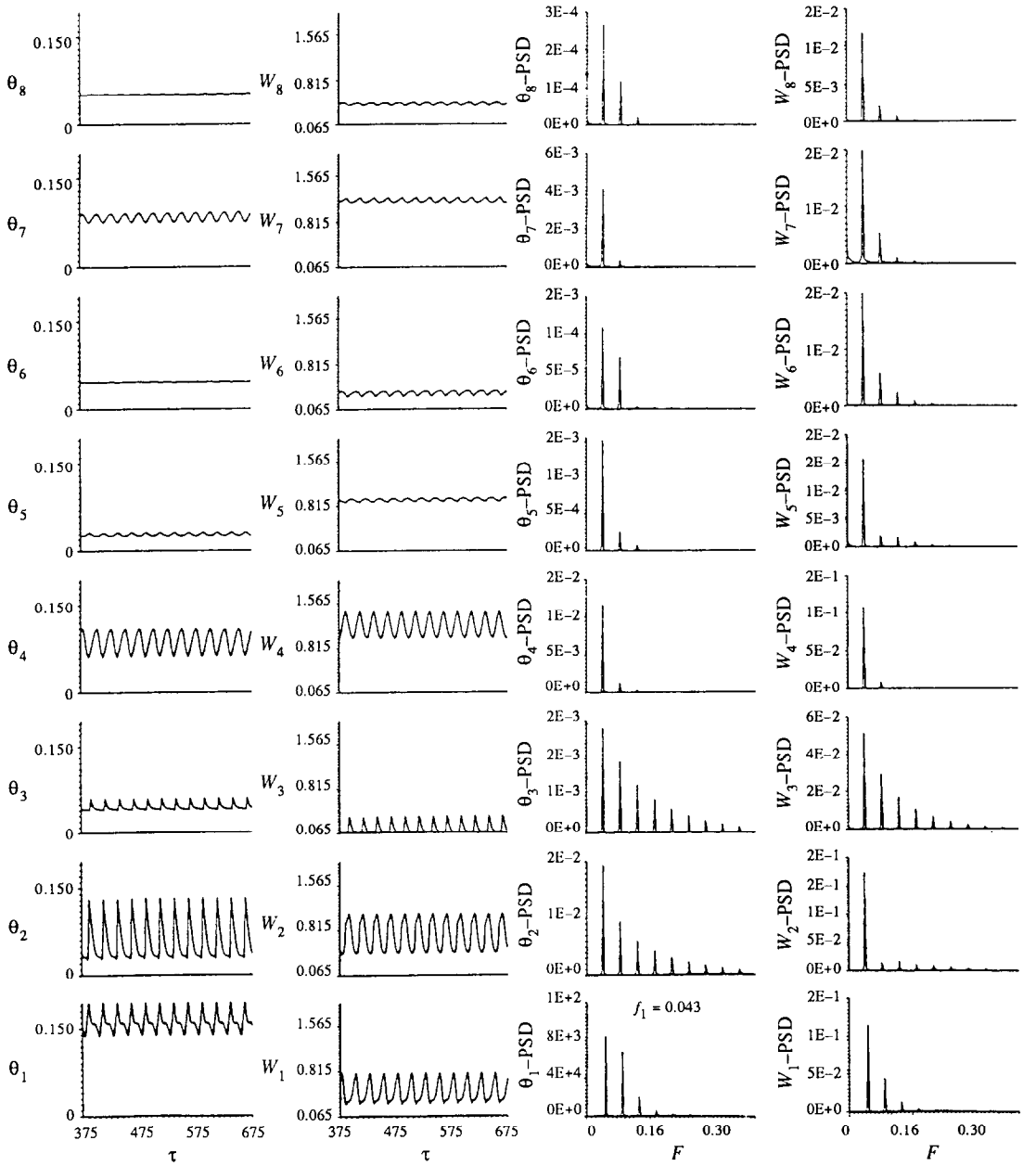

FIG. 7. Time histories and power spectrum densities at eight detection points for W and Θ for $Pr = 0.72$, $Re = 500$, $Gr/Re^2 = 5$, $A = 2$ and $L = 20$ at $Z = 14.84$. (Θ_i and W_j respectively denote Θ and W at detection points i and j.)

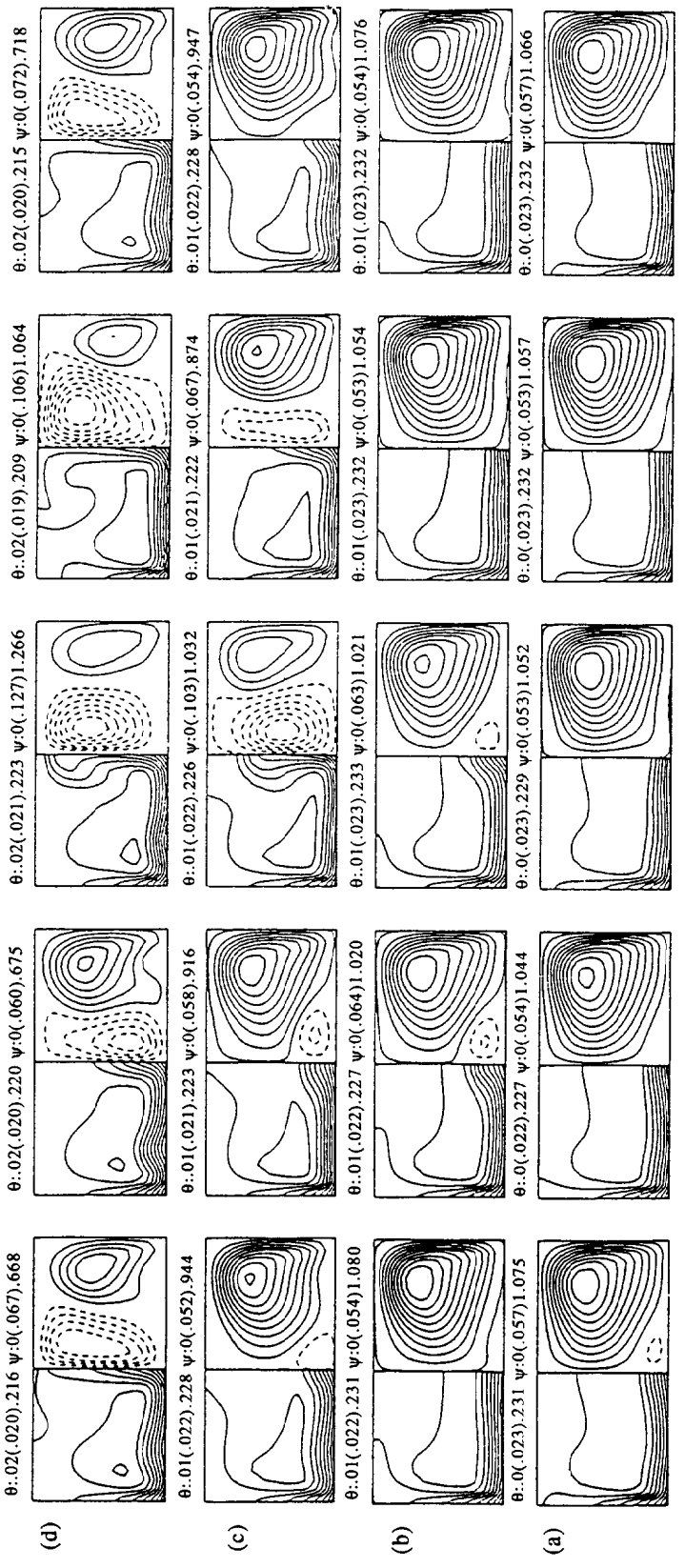

FIG. 8. Secondary flow patterns in a typical period at large τ for $Gr/Re^2 = 5$ at $Z =$ (a) 9.03, (b) 11.61, (c) 14.19, (d) 16.77. The period of the oscillation is about 24.

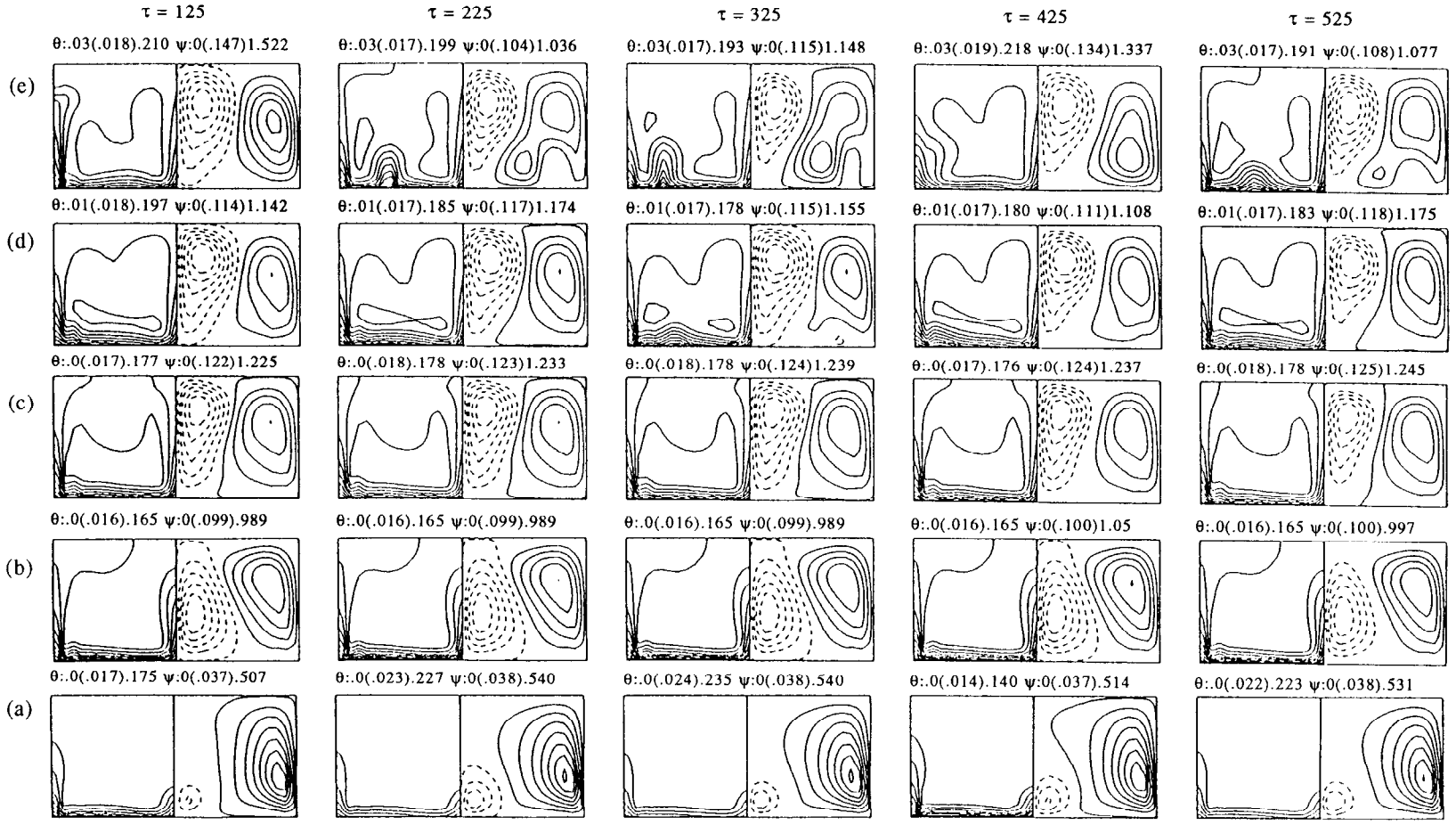

FIG. 9. Isotherms and cross-sectional streamlines for $Gr/Re^2 = 10$ at (a) $Z = 1.29$, (b) $Z = 3.87$, (c) $Z = 6.45$, (d) $Z = 9.03$, (e) $Z = 11.61$ for $\tau = 125$, 225, 325, 425 and 525.

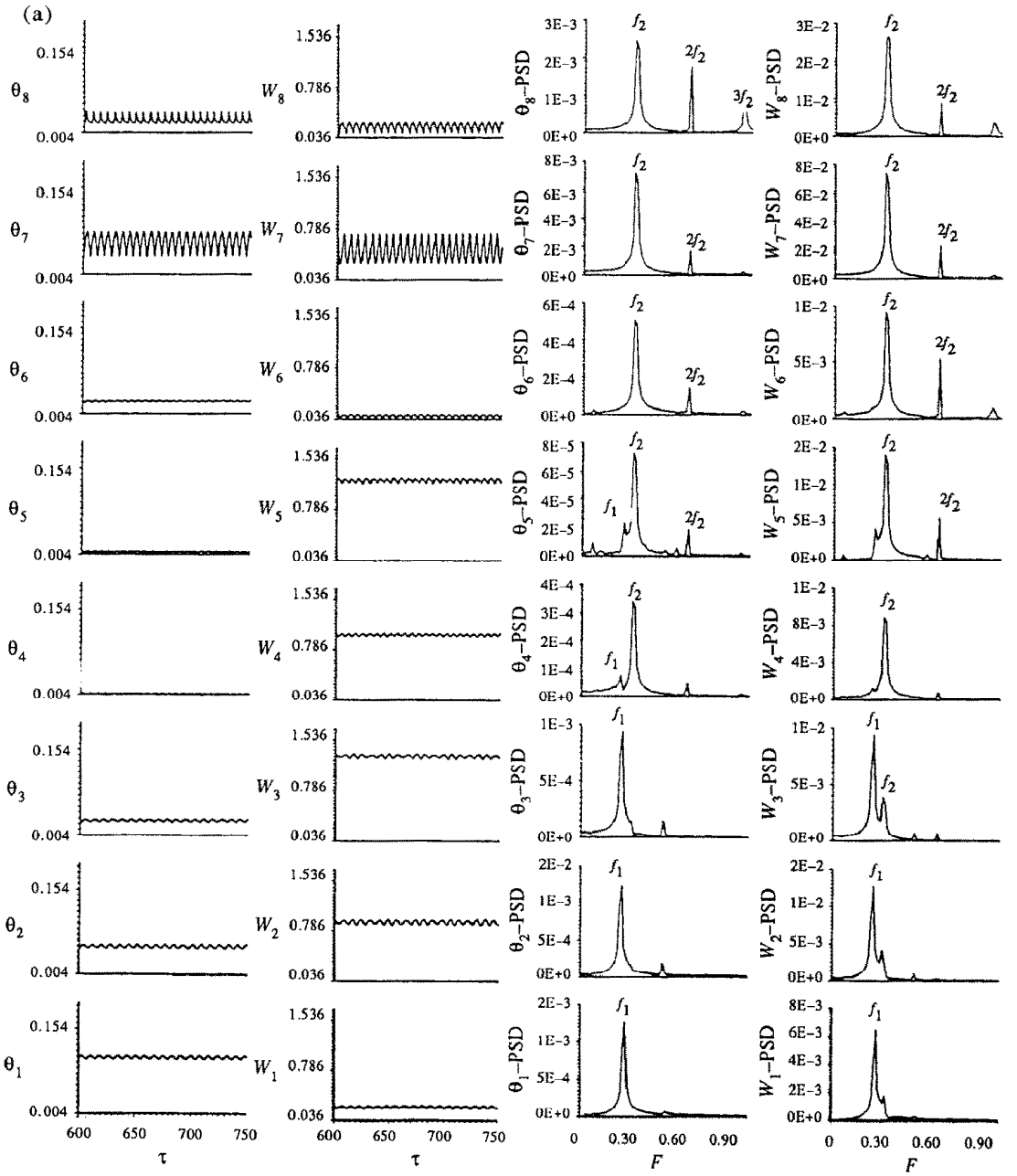

FIG. 10. Time records of Θ and W and the corresponding power spectrum densities at selected detection points for $Gr/Re^2 = 30$ at cross sections (a) $Z = 3.23$, (b) $Z = 7.10$, and (c) $Z = 18.70$. ($f_3 = f_1 + 3/4f_2$, $f_4 = 1/4f_1$, $f_5 = 5/4f_1 + 3/4f_2$, $f_6 = f_1 - 1/2f_2$, $f_7 = f_1 + 1/2f_2$, $f_8 = 3/4f_1 + 1/8f_2$, $f_9 = 5/4f_1 + 3/4f_2$, $f_{10} = 3/4f_2, f_{11} = 3f_2$.)

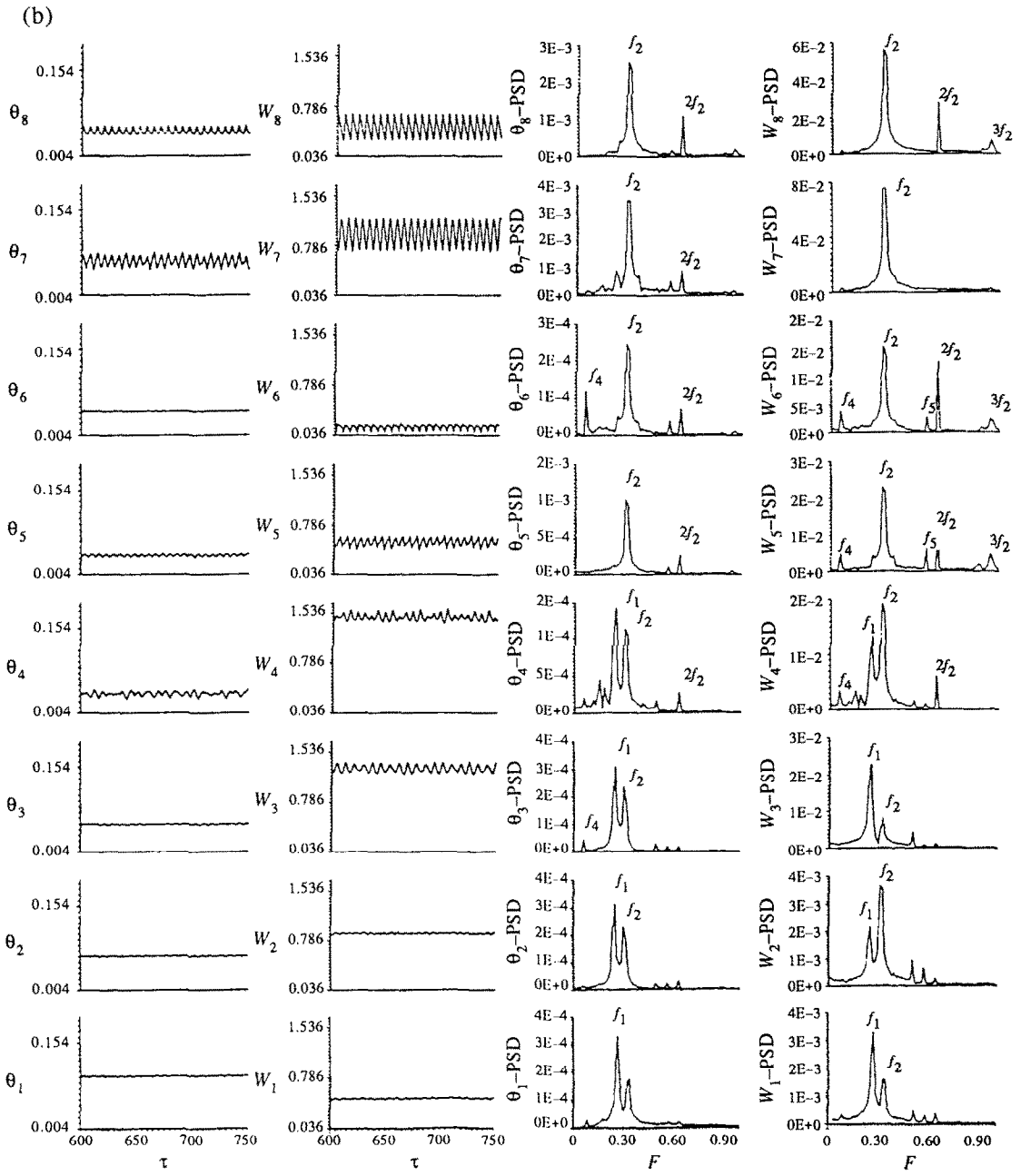

FIG. 10—*continued.*

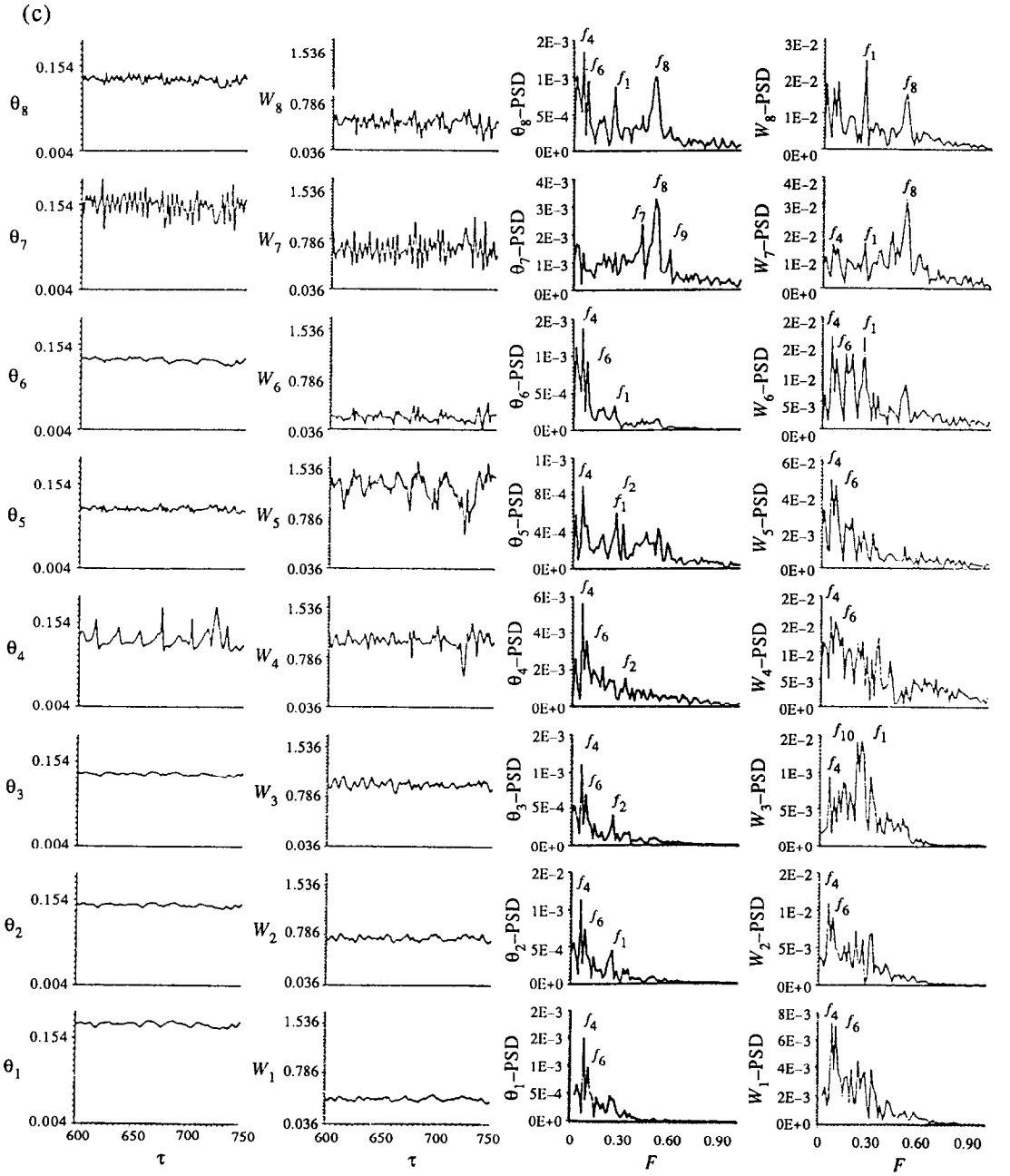

FIG. 10—*continued.*

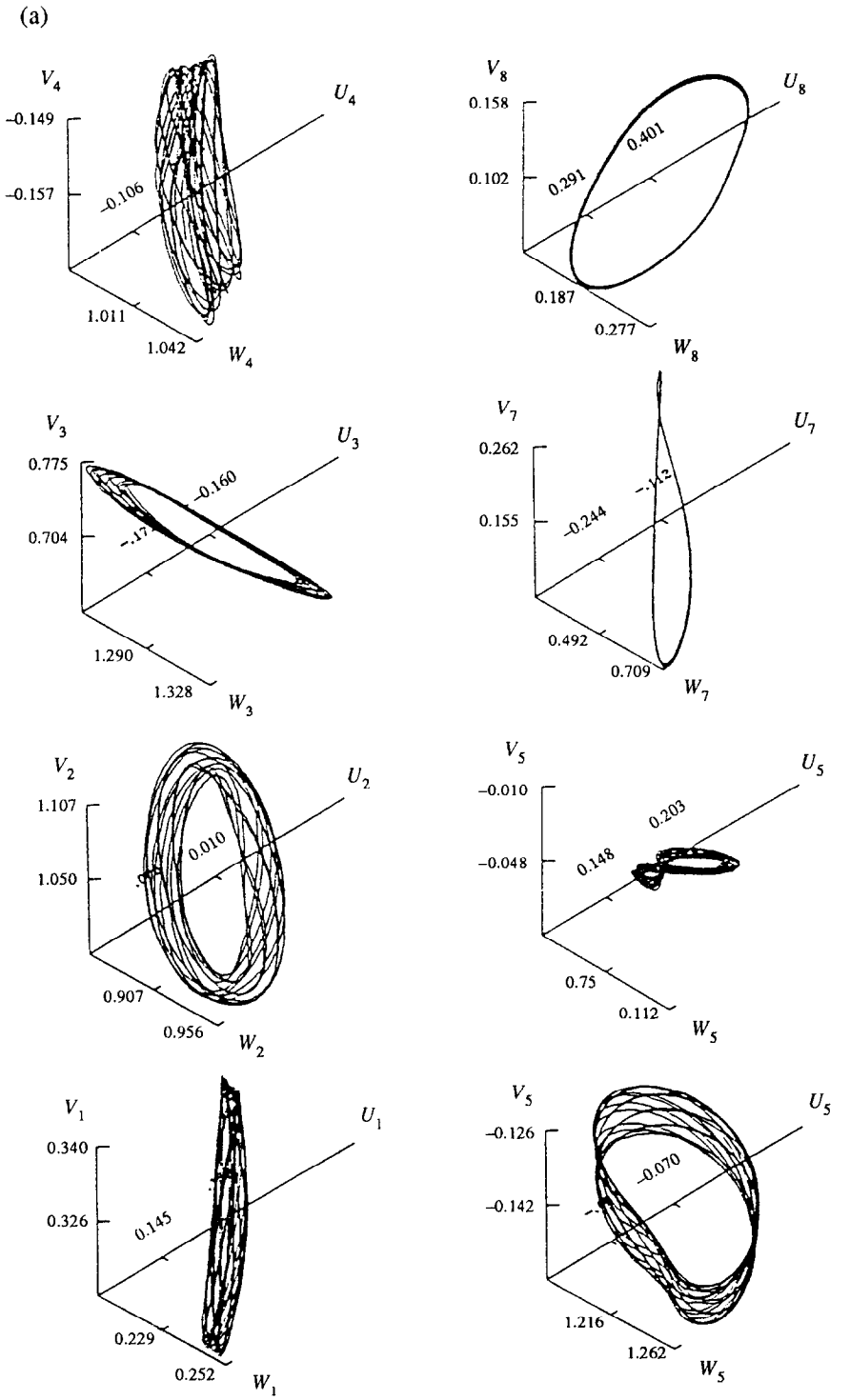

FIG. 11. Phase space trajectories of the velocity components U, V and W at selected points for $Gr/Re^2 = 30$ at cross sections (a) $Z = 3.23$ and (b) $Z = 7.10$.

(b)

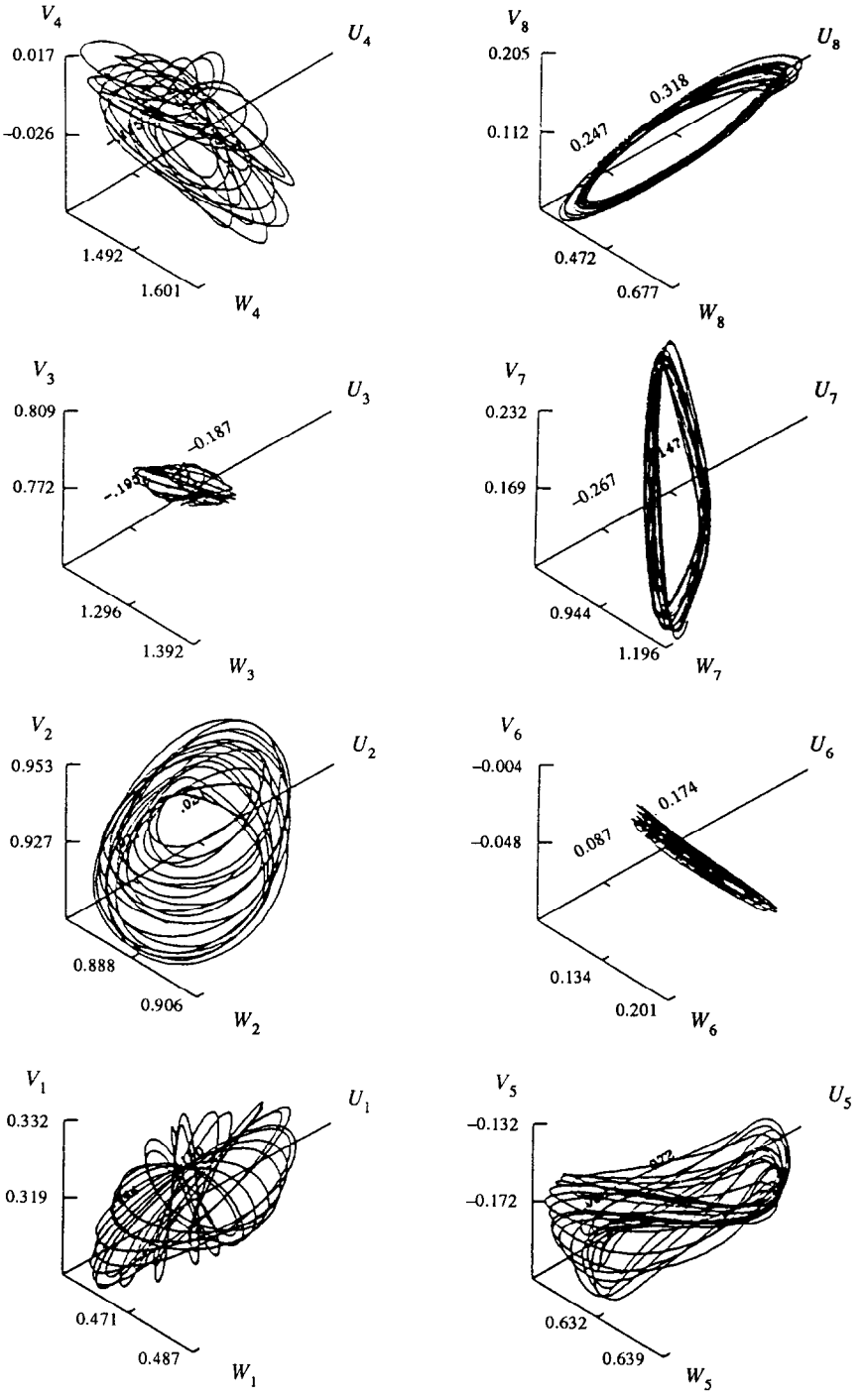

FIG. 11—*continued.*

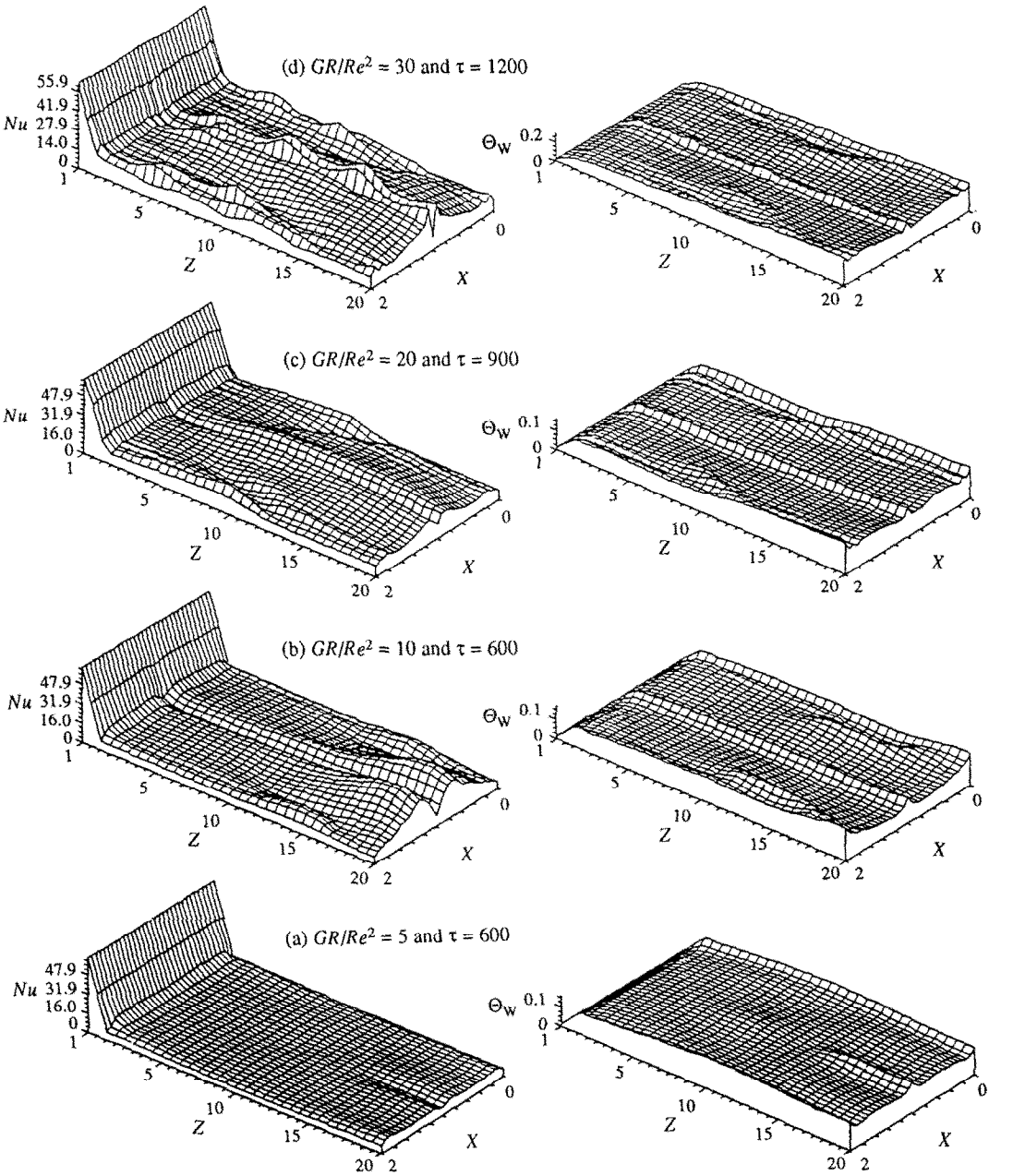

FIG. 12. The local Nusselt number distributions on the heated bottom plate for various Gr/Re^2 at large τ.

wall region is quasiperiodic and the core flow exhibits some irregularity but with distinct structure (Figs. 10(b) and 11(b)). In particular, at locations 1 and 5 each cycle in the phase diagram is like a butterfly which gradually rotates laterally around a certain axis. Further downstream near the exit of the heated section at $Z = 18.70$ the flow is entirely chaotic with relatively irregular temperature and velocity signals with the banded PSDs.

To further enhance our understanding of the overall flow development, the flow fields for this high buoyancy case were carefully examined. It is of interest to note the significant axial decay and growth of the longitudinal rolls. Near the exit of the heated section the rolls in the core region are smaller in size and fluctuate in a smaller amplitude. Furthermore, the thermal boundary layer on the heated plate is unstable and prevailed by the travelling waves resulting from the strong upward buoyancy.

Results for the local Nusselt number distribution over the heated plate are of value in thermal system design. Figure 12 presents these results for $Gr/Re^2 = 5, 10, 20$ and 30 at large τ. In the entry region significant reduction in Nu with the axial distance is noted for various Gr/Re^2 reflecting the flow being dominated by forced convection. A close inspection, however, discloses that noticeable spanwise variations due to upward thermal buoyancy already appear in this entry region especially at higher Gr/Re^2. Downstream of the entry region Nu levels off somewhat in Z direction over some distance before it significantly rises but the spanwise variations resulting from the presence of the longitudinal rolls become relatively substantial especially for $Gr/Re^2 = 30$. This distance is shorter at a higher Gr/Re^2. Due to the nonmonotonic axial variations in the secondary flow intensity the axial variations of Nu are also nonmonotonic. Thus a complicated instantaneous Nu distribution at $Gr/Re^2 = 30$ results (Fig. 12(d)).

Some important characteristics of the fluctuating flow for selected cases are summarized in Table 1. In the table $(Z^+)_{hf}$ is the location where the Hopf bifurcation (periodic flow oscillation) is first observed. A flow is considered as undergoing a Hopf bifurcation when the oscillation amplitude in the local Nusselt number at any location on the heated plate exceeds 3% of the steady value before the oscillation at that location. Also included in the table are the fundamental modes of the velocity and temperature oscillations at large times. Finally, the amplitudes of the oscillations at detection points 1, 4, 5, and 7 at cross sections $Z = 7.10$ and 14.83 are given. Note that for flow characterized by a single fundamental frequency ($Gr/Re^2 < 19$) the frequency increases with Gr/Re^2. No simple trend, however, can be identified when the second fundamental mode appears for $Gr/Re^2 \geqslant 19$. The selected data for the oscillation amplitudes of W and Θ at long time given here again emphasize the flow oscillation being substantially position dependent without any simple relation with the downstream distance and the mixed convection parameter Gr/Re^2, as mentioned earlier. An empirical correlation is proposed to fit the calculated Hopf Bifurcation point

$$Ra^* = 8413(Z^+)^{-1.26}. \tag{20}$$

This bifurcation point is found to locate downstream

Table 1. Effects of Gr/Re^2 on the Hopf bifurcation, fundamental frequencies and amplitudes of Θ and W oscillations at large τ

Gr/Re^2	Z^+_{hf}	f_1 f_2	$Z = 7.10$ $A(\Theta_1), A(\Theta_4), A(\Theta_5), A(\Theta_7)$ $A(W_1), A(W_4), A(W_5), A(W_7)$	$Z = 14.83$ $A(\Theta_1), A(\Theta_4), A(\Theta_5), A(\Theta_7)$ $A(W_1), A(W_4), A(W_5), A(W_7)$
4.0	0.0380	$f_1 = 0.030$	0.000, 0.000, 0.000, 0.000	0.012, 0.000, 0.000, 0.000
			0.000, 0.000, 0.000, 0.001	0.060, 0.035, 0.035, 0.010
5.0	0.0220	$f_1 = 0.043$	0.010, 0.003, 0.000, 0.002	0.060, 0.050, 0.007, 0.017
			0.060, 0.019, 0.003, 0.007	0.440, 0.400, 0.065, 0.090
8.0	0.0160	$f_1 = 0.060$	0.000, 0.000, 0.000, 0.000	0.008, 0.100, 0.033, 0.095
			0.000, 0.002, 0.001, 0.003	0.014, 0.620, 0.100, 0.700
10.0	0.0130	$f_1 = 0.075$	0.000, 0.004, 0.000, 0.006	0.014, 0.070, 0.050, 0.080
			0.001, 0.025, 0.005, 0.030	0.030, 0.750, 0.580, 0.800
15.0	0.0086	$f_1 = 0.120$	0.001, 0.005, 0.004, 0.070	0.001, 0.009, 0.005, 0.050
			0.005, 0.060, 0.120, 0.850	0.022, 0.140, 0.350, 0.320
19.0	0.0081	$f_1 = 0.137$	0.001, 0.008, 0.005, 0.060	0.001, 0.004, 0.008, 0.030
		$f_2 = 0.203$	0.006, 0.120, 0.160, 0.880	0.030, 0.120, 0.120, 0.380
20.0	0.0073	$f_1 = 0.130$	0.001, 0.060, 0.006, 0.070	0.008, 0.400, 0.800, 0.055
		$f_2 = 0.143$	0.012, 0.600, 0.050, 0.800	0.070, 0.040, 0.800, 0.550
30.0	0.0067	$f_1 = 0.266$	0.003, 0.015, 0.007, 0.025	0.006, 0.015, 0.017, 0.050
		$f_2 = 0.320$	0.030, 0.170, 0.200, 0.480	0.060, 0.200, 0.650, 0.550
35.0	0.0066	$f_1 = 0.200$	0.003, 0.010, 0.008, 0.050	0.004, 0.008, 0.006, 0.002
		$f_2 = 0.280$	0.060, 0.150, 0.550, 0.550	0.040, 0.140, 0.300, 0.220

Note: where $A(\Theta_i)$ and $A(W_i)$ are respectively the oscillation amplitudes of temperature Θ and velocity component W at the detection point i at large τ.

of the position where the vortex rolls are first induced, the so called 'Onset of Secondary Flow'.

CONCLUDING REMARKS

The effects of the buoyancy-to-inertia force ratio Gr/Re^2 on the unsteady and transitional characteristics of the mixed convection flow of air ($Pr = 0.72$) in a bottom heated horizontal rectangular duct are numerically investigated for $Re = 500$ and $A = 2$. The results indicate that as $Gr/Re^2 < 4$ the flow is dominated by two steady longitudinal rolls near the side wall. As $4 \leqslant Gr/Re^2 < 19$ the flow becomes unsteady after certain critical axial distance from the inlet. This critical distance is shorter for a higher Gr/Re^2 and the unsteady flow characterized by four longitudinal rolls is time periodic with a single fundamental frequency along with its harmonics. Then, as $19 \leqslant Gr/Re^2 < 25$ the flow is steady only in a very small region near the inlet. The unsteady flow in the downstream region is nonperiodic and characterized by two incommensurate frequencies and their linear combinations. For $Gr/Re^2 \geqslant 25$ the flow is chaotic in the exit region near the trailing edge of the heated plate. The above results suggest that the buoyancy induced flow transition follows the Ruelle–Taken route [43].

Acknowledgement—The financial support of this study by the engineering division of Nation Science Council of Taiwan, R.O.C. through the contract NSC79-0401-E009-18 is greatly appreciated.

REFERENCES

1. W. M. Kays and A. L. London, *Compact Heat Exchangers* (3rd Edn). McGraw-Hill, New York (1984).
2. F. P. Incropera, Convective heat transfer in electronic equipment cooling, *J. Heat Transfer* **110,** 1097–1111 (1988).
3. G. Evan and R. Grief, A study of traveling wave instabilities in a horizontal channel flow with applications to chemical vapor deposition, *Int. J. Heat Mass Transfer* **32,** 895–911 (1989).
4. Y. Mori and Y. Uchida, Forced convective heat transfer between horizontal flat plates, *Int. J. Heat Mass Transfer* **9,** 803–817 (1966).
5. M. Akiyama, G. J. Hwang and K. C. Cheng, Experiments on the onset of longitudinal vortices in laminar forced convection between horizontal plates, *J. Heat Transfer* **93,** 335–341 (1971).
6. S. Ostrach and Y. Kamotani, Heat transfer augmentation in laminar fully developed channel flow by means of heating from below, *J. Heat Transfer* **97,** 220 225 (1975).
7. Y. Kamotani and S. Ostrach, Effect of thermal instability on thermally developing laminar channel flow, *J. Heat Transfer* **98,** 62–66 (1976).
8. G. J. Hwang and C. L. Liu, An experimental study of convective instability in the thermal entrance region of a horizontal parallel-plate channel heated from below, *Can. J. Chem. Engng* **54,** 521–525 (1976).
9. Y. Kamotani, S. Ostrach and H. Miao, Convective heat transfer augmentation in thermal entrance regions by means of thermal instability, *J. Heat Transfer* **101,** 222–226 (1979).
10. K. C. Chiu and F. Rosenberger, Mixed convection between horizontal plates—I. Entrance effects, *Int. J. Heat Mass Transfer* **30,** 1645–1654 (1987).
11. K. C. Chiu, J. Ouazzani and F. Rosenberger, Mixed convection between horizontal plates—II. Fully developed flow, *Int. J. Heat Mass Transfer* **30,** 1655–1662 (1987).
12. M. T. Ouazzani, J. P. Caltagironc, G. Meyer and A. Mojtabi, Etude numérique et expérimental de la convection mixte entre deux plans horizontaux, *Int. J. Heat Mass Transfer* **32,** 261–269 (1989).
13. M. T. Ouazzani, J. K. Platten and A. Mojtabi, Etude expérimental de la convection mixte entre deux plans horizontaux à températures différents—II, *Int. J. Heat Mass Transfer* **33,** 1417–1427 (1990).
14. D. G. Osborne and F. P. Incropera, Laminar, mixed convection heat transfer for flow between horizontal parallel plates with asymmetric heating, *Int. J. Heat Mass Transfer* **28,** 207–217 (1985).
15. D. G. Osborne and F. P. Incropera, Experimental study of mixed convection heat transfer for transitional and turbulent flow between horizontal, parallel plates, *Int. J. Heat Mass Transfer* **28,** 1337–1344 (1985).
16. F. P. Incropera, A. L. Knox and J. A. Schutt, Onset of thermally driven secondary flow in horizontal rectangular ducts, *Proc. 8th Int. Heat Transfer Conf.*, San Francisco, pp. 1395–1400 (1986).
17. F. P. Incropera, A. L. Knox and J. R. Maughan, Mixed-convection flow and heat transfer in the entry region of a horizontal rectangular duct, *J. Heat Transfer* **109,** 434–439 (1987).
18. J. R. Maughan and F. P. Incropera, Experiments on mixed convection heat transfer for airflow in a horizontal and inclined channel, *Int. J. Heat Transfer* **30,** 1307–1318 (1987).
19. J. R. Maughan and F. P. Incropera, Regions of heat transfer enhancement for laminar mixed convection in a parallel plate channel, *Int. J. Heat Mass Transfer* **33,** 555–570 (1990).
20. W. Nakayama, G. J. Hwang and K. C. Cheng, Thermal instability in plane Poiseuille flow, *J. Heat Transfer* **92,** 61–68 (1970).
21. G. J. Hwang and K. C. Cheng, Convective instability in the thermal entrance region of a horizontal parallel-plate channel heated from below, *J. Heat Transfer* **95,** 72–77 (1973).
22. F. S. Lee and G. J. Hwang, Transient analysis on the onset of thermal instability in the thermal entrance region of a horizontal parallel plate channel, *J. Heat Transfer* **113,** 363–370 (1991).
23. K. C. Cheng and G. J. Hwang, Numerical solution for combined free and forced laminar convection in horizontal rectangular channels, *J. Heat Transfer* **91,** 59–66 (1969).
24. K. C. Cheng, S. W. Hong and G. J. Hwang, Buoyancy effects on laminar heat transfer in the thermal entrance region of horizontal rectangular channels with uniform wall heat flux for large Prandtl number fluid, *Int. J. Heat Mass Transfer* **15,** 1819–1836 (1972).
25. J. W. Ou, K. C. Cheng and R. C. Lin, Natural convection effects on Graetz problem in horizontal rectangular channels with uniform wall temperature for large *Pr*, *Int. J. Heat Mass Transfer* **15,** 835–843 (1974).
26. K. C. Cheng and J. W. Ou, Convective instability and finite amplitude convection in the thermal entrance region of horizontal rectangular channels heated from below, *Proc. 7th Int. Heat Transfer Conf.*, Munich, Germany, Paper NC-12, pp. 189–194 (1982).
27. K. C. Cheng and J. W. Ou, Buoyancy and tilt angle effects on Graetz problem in horizontal rectangular channels, *Proc. ASME–JSME Joint Conf. on Thermal Engng*, Vol. **3,** pp. 141–147 (1983).
28. F. C. Chou and G. J. Hwang, Vorticity–velocity method

for the Graetz problem and the effect of natural convection in a horizontal rectangular channel with uniform wall heat flux, *J. Heat Transfer* **109,** 704–710 (1987).
29. G. J. Hwang and F. C. Chou, Effect of wall conduction on combined free and forced laminar convection in horizontal rectangular channels, *J. Heat Transfer* **109,** 936–942 (1987).
30. F. C. Chou and W. Y. Lien, Effect of wall heat conduction on laminar mixed convection in the thermal entrance region of horizontal rectangular channels, *Wärme- und Soffübertragung* **26,** 121–127 (1991).
31. J. M. Huang, J. D. Lin and F. C. Chou, Combined radiation and laminar mixed convection in the thermal entrance region of horizontal isothermal rectangular channels, *Numer. Heat Transfer A* **18,** 113–125 (1990).
32. F. P. Incropera and J. A. Schutt, Numerical simulation of laminar mixed convection in the entrance region of horizontal rectangular ducts, *Numer. Heat Transfer* **8,** 707–729 (1985).
33. H. V. Mahaney, F. P. Incropera and S. Ramadhyani, Development of laminar mixed convection flow in a horizontal rectangular duct with uniform bottom heating, *Numer. Heat Transfer* **12,** 137–155 (1987).
34. H. V. Mahaney, F. P. Incropera and S. Ramadhyani, Effect of wall heat flux distribution on laminar mixed convection in the entrance region of a horizontal rectangular duct, *Numer. Heat Transfer* **13,** 427–450 (1988).
35. H. V. Mahaney, S. Ramadhyani and F. P. Incropera, Numerical simulation of three-dimensional mixed convection heat transfer from an array of discrete heat sources in a horizontal rectangular duct, *Numer. Heat Transfer A* **16,** 267–286 (1989).
36. J. R. Maughan and F. P. Incropera, Fully developed mixed convection in a horizontal channel heated uniformly from above and below, *Numer. Heat Transfer A* **17,** 417–430 (1990).
37. R. K. Shah and A. L. London, *Laminar Flow Force Convection in Ducts*, pp. 196–198. Academic Press, New York (1978).
38. A. J. Chorin, Numerical solution of the Navier–Stokes equations, *J. Math. Comp.* **22,** 742–762 (1968).
39. R. Peyret and T. D. Taylor, *Computational Methods for Fluid Flow* (Chap. 6). Springer, New York (1983).
40. T. Kawamura, H. Takami and K. Kuwahara, New higher-order upwind scheme for incompressible Navier–Stokes equations, *9th ICNMFD* **10,** 285–291 (1985).
41. C. Hirsch, *Numerical Computation of Internal and External Flow*, Vol. 1, pp. 176–179. Wiley New York (1989).
42. D. A. Anderson, J. C. Tannehill and R. H. Pletcher, *Computational Fluid Mechanics and Heat Transfer*, pp. 71–77. Hemisphere, Washington, DC (1984).
43. J. Argyris, G. Faust and M. Haase, An adventure in chaos, *Comp. Meth. Appl. Mech. Engng* **91,** 997–1091 (1991).